Rocket Combustion Modelling
Test Case RCM-3
*
Numerical calculation of MASCOTTE 60 bar case with THESEE

A. Depoutre, S. Zurbach, D. Saucereau, J.P. Dumont
SNECMA Moteurs

E Bodèle, I. Gökalp
LCSR

Introduction

This paper presents the numerical simulation of the RCM-3 test case done by Snecma and LCSR. The specified inlet conditions and computational options are described in the paper. A brief discussion about the main results is also given.

Operating point

The MASCOTTE operating point to be simulated was given by the workshop specifications. It is defined in the following table:

RCM-3			
Pressure	RM	$\dot{m}$ (LOX)	$\dot{m}$ (GH2)
60 bar	1,4	100 g/s	70 g/s

Numerical simulation

The code used to perform the calculation is a RANS code called THESEE. This solver enables the computation of 2D or 3D geometries with unstructured multi-element meshes. It can predict multiphase, multispecies turbulent reactive flows under steady or unsteady condition. The numerical scheme is based on a finite volume formulation for the Navier-Stokes equations.

The calculation was performed with the following assumptions:

- Compressible reactive flow
- Standard k - ε turbulence model
- EBU combustion model
- Unsteady and fully coupled lagrangian droplet tracking
- Evaporation rate estimated by the Delplanque-Sirignano model
- Ideal gas law with variable thermodynamics
- Variable thermodynamic properties for the droplets

Three different gaseous species were considered: H_2, O_2, H_2O and one liquid specie: liquid oxygen. The gaseous phase and the liquid phase are solved in the same time, in a coupled manner. We assumed variables thermodynamic properties for the four species and a single chemical reaction (H_2O):

$$H_2 + 1/2\ O_2 \rightarrow \text{Products } (H_2O + \text{dissociation})$$

It should be noticed that the Cv of the third specie H2O was corrected to take into account the dissociation processes occurring at high temperature in order to avoid an overestimation of the adiabatic flame temperature.

All gaseous properties, μ (viscosity) and λ (conductivity) are functions of the temperature. For the liquid oxygen, the variations due to the temperature for the Cp, μ, Hvap (enthalpy of vaporisation) , ρ (density), σ (surface tension) and Yos (gaseous oxygen mass fraction on the droplet surface) were also taken into account.

The numerical options are the following :

- 2D axi symmetric computation
- Unstructured hexahedrons mesh
- ALE scheme for the two-phase flow
- Explicit convection 2nd order

Geometry and grid

The computation was performed on a 2D axisymmetric geometry consisting of a 20° slice (length 400 mm, radius 25 mm) of the chamber. The nozzle was not modelled and so we assumed a constant pressure in the chamber. The computational domain ends at the exit of the cylindrical combustor at x = 400 mm.

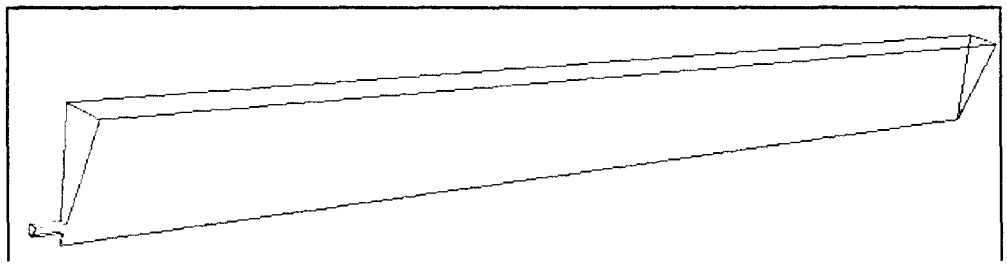

Geometry of the simulation

We use an unstructured hexahedrons mesh of 5373 cells.

Unstructured hexahedrons mesh

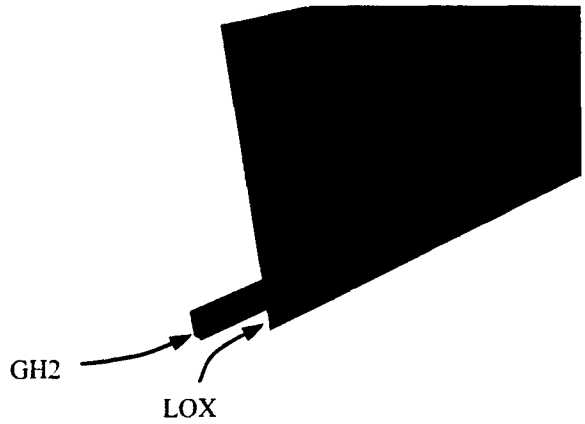

Inlet boundary condition

Boundary conditions

Hydrogen injection: Gaseous hydrogen was injected through the annular injector. This inflow is subsonic and the total temperature and mass flow rate were specified.

Oxygen injection: Droplets were injected in the axial direction through a porous wall, with a random position, as required in the RCM3 specification. The injection droplet velocity was increased to 20 m/s to avoid droplet accumulation in the recirculation zone behind the lox inlet. We chose a macro-droplet weight equal to 10 to reduce the total number of physical droplets.

Exit area: As the nozzle was not considered, the outflow is subsonic and the outlet conditions are determined by fixing the static pressure.

Boundary conditions		
Hydrogen inlet	Droplet injection	Outlet
$\dot{m}$ = 70 g/s T = 287 K P = 60 bar V = 236 m/s	$\dot{m}$ = 100 g/s T = 85 K V = 20 m/s Macro-droplet weight = 10 Size D32 = 50 µm	P = 60 bar Y_{H_2} = 0.344 Y_{O_2} = 0 Y_{H_2O} = 0.656

Walls : Slip conditions were used and the combustion chamber walls are assumed to be adiabatic.

Initial condition

The combustion chamber is initialised with hydrogen at 287 K.

Results

The total CPU time necessary to obtain the converged was about 180 hours. The calculation was performed with the Delplanque-Sirignano evaporation rate model without stripping.

The velocity fields in Fig.1 and 2 exhibit a deviation of the hydrogen jet due to atomisation and combustion. A recirculation zone is located between the injector and the upper and lower walls. This recirculation contains about 70% of gaseous hydrogen, 30% of water vapour and no gaseous oxygen (see Fig. 5, 6 and 7). The temperature in the recirculation is about 900 K (Fig. 3).

Figures 9 and 10 show the mean reaction rate field. The flame length is about 230 mm. Figure 10 shows three characteristic structures of a cryogenic flame :

- A first expansion cone of length L_1 = 15×Dlox. This zone is the longest one and its expansion is weak.
- A second expansion zone of length (L2-L1) with L2 = 19×Dlox. This zone is shorter than the first one, but its expansion is higher due to the recirculation zone and the attachment point.
- A confining zone where the flame ends and parabolic temperature profiles.

The temperature fields (Fig.3) give an estimation of the flame position and length. Assuming a "mixed is burnt" type model, the flame is attached to the injector tip. The maximum mean temperature is about 3600 K and the outlet averaged temperature is about

1600 K. This result can be compared to the temperature computed by an equilibrium code , minimising the Gibbs free energy ;for RM 1.4,the equilibrium temperature is equal to the 1580 K.

The mean mass fraction fields are presented on figures 5, 6 and 7. The outlet H2O fraction integrated on the outlet is about 0.66 (Fig.8). This value is similar to the equilibrium one at RM 1.4 and equal to 0.656.

Figures 11, 12 and 13 are the prediction of the velocity, temperature and droplet diameter fields.

Compared to the available experimental data of fig 14 and 15, the global structure of the flame is therefore correctly represented, particularly on the observed attachment point due to the combustor confinement and the corresponding recirculation effect. Also, the initial angle of the flame is close to the experimental data. However, there is a discrepency between the calculation and the observed length of the flame, certainly due to the choice made on the drop size and initial velocity.

Conclusion

The numerical computation of the 2D axisymmetric MASCOTTE configuration at RCM-3 operating point was presented.

At 60 bars, the liquid oxygen is fully consumed in the chamber and the global structure of the flame is correctly represented. However, the computed flame length is longer than the experimental data. This phenomenon is due to the droplets injection velocity which has been increased to 20 m/s to avoid accumulation of droplets downstream of the porous wall injection. It was the biggest difficulty we have encountered in our simulations and a solution would be to simulate the droplets injection boundary condition from a potential cone.

Moreover, we don't consider stripping in the evaporation rate model, and this approach could affect the length of the flame. It is also clear that a lagrangien model is not ideal for such type of high pressure simulation and that a real fluid modelization would be better suited. Finally, more experimental measurements should be available and compared in detail with calculation results.

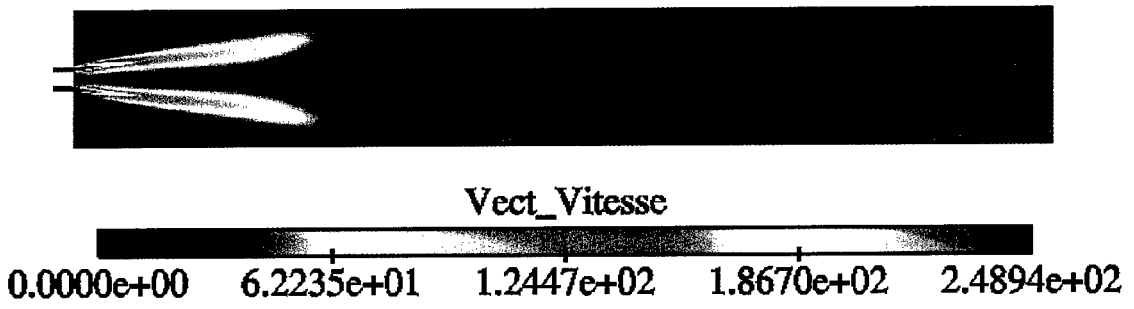

Fig. 1: Contours of velocity (m/s)

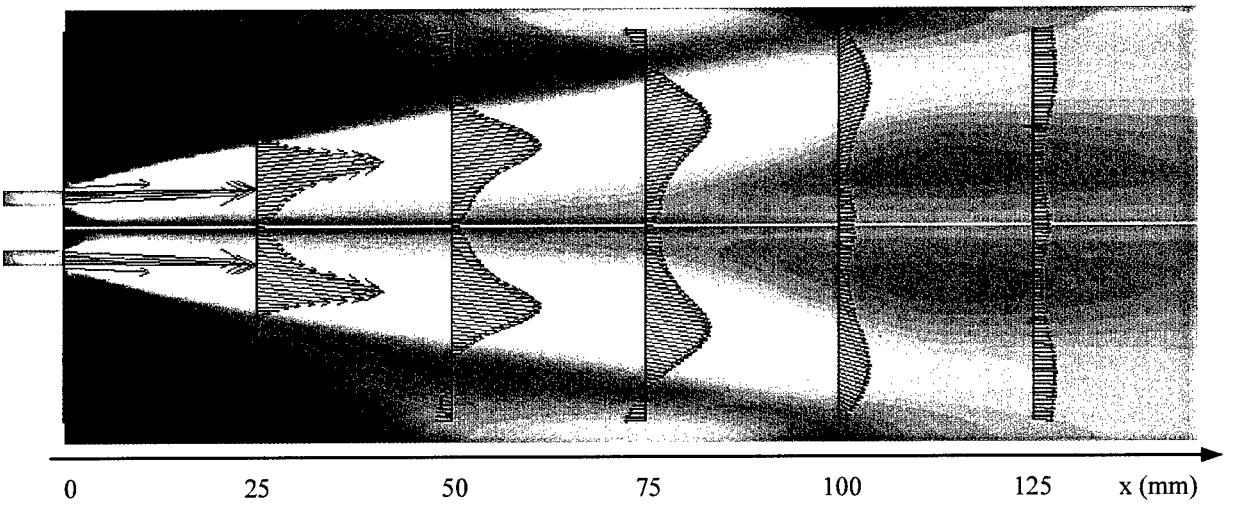

Fig. 2: Field and profiles of velocity vectors

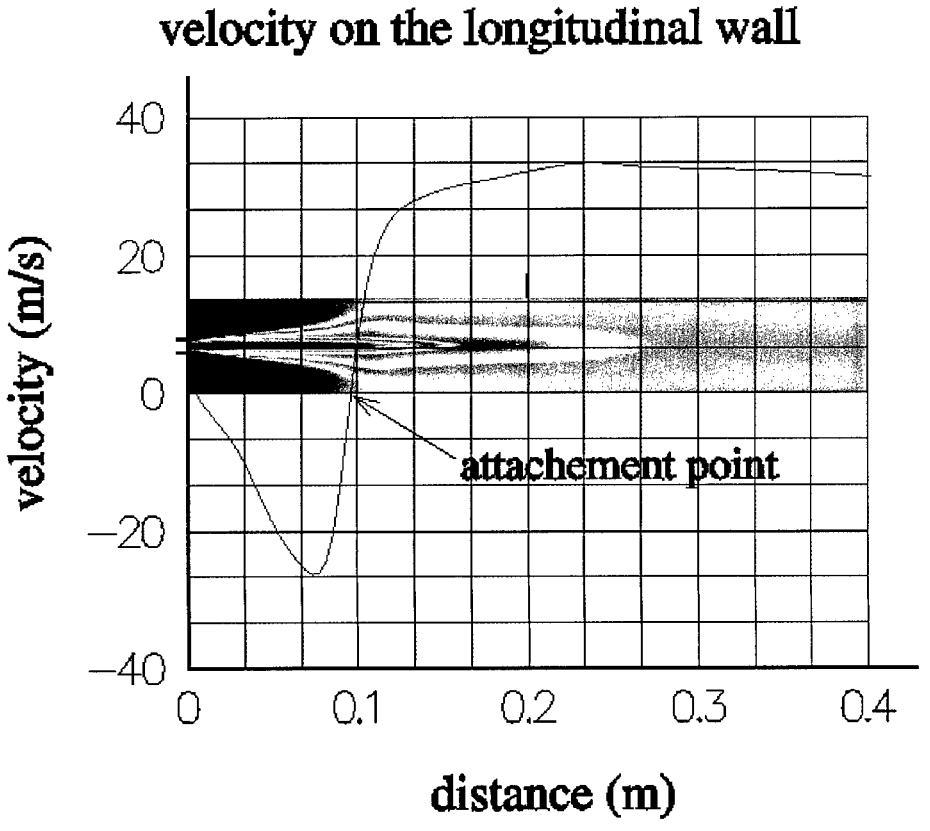

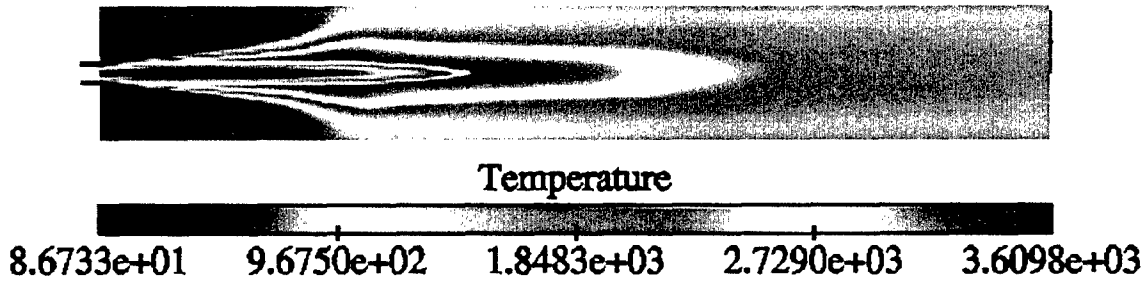

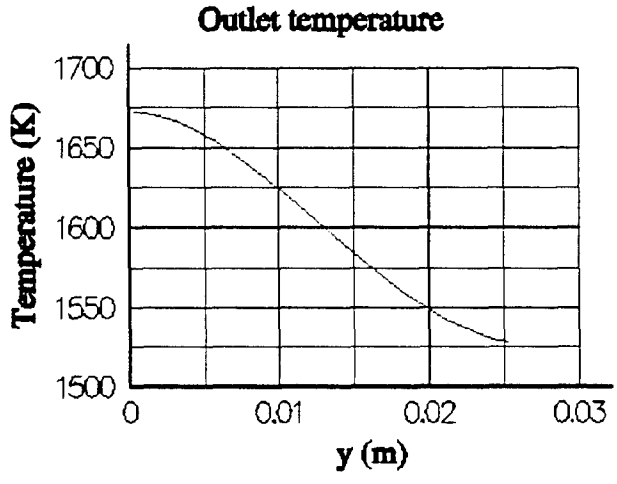

Fig. 3: Mean temperature fields (K)

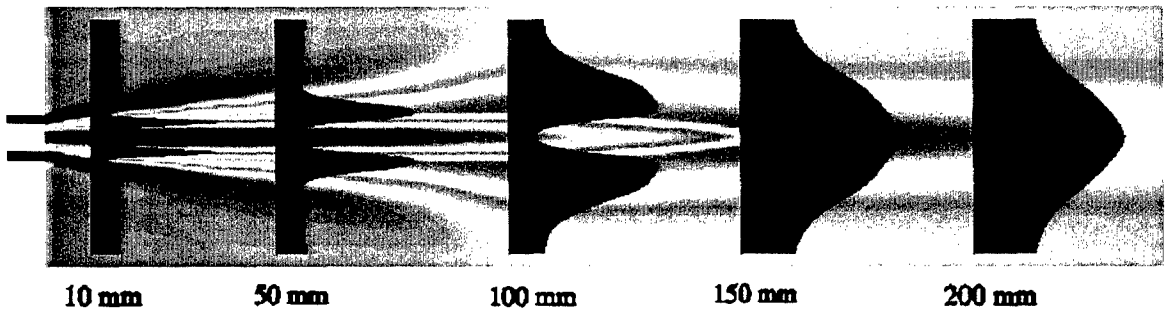

Fig. 4: Field and Radial Temperature profiles

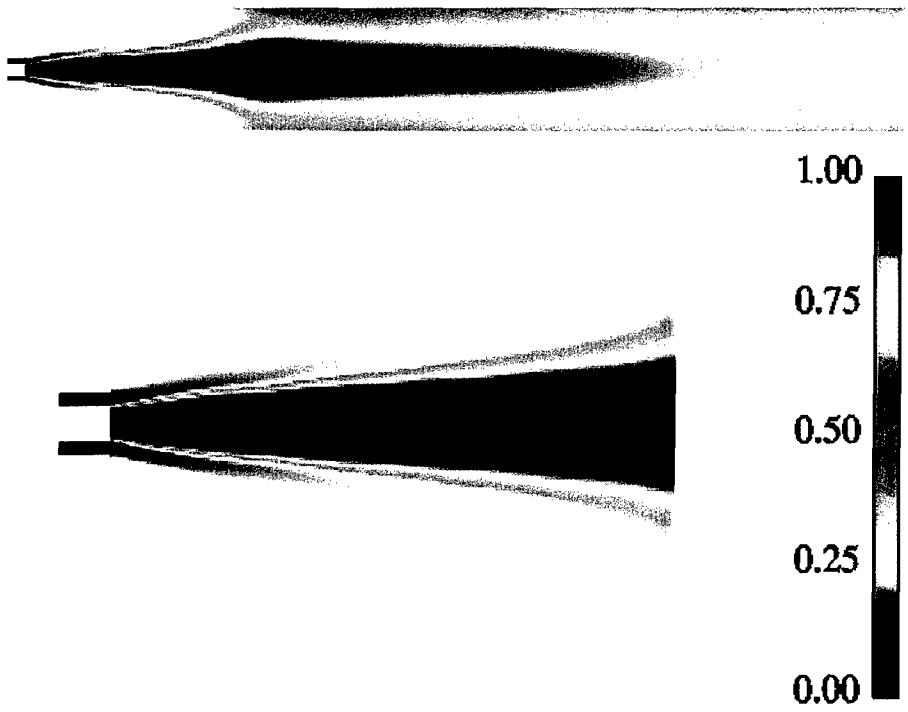

Fig. 5: Gaseous Hydrogen mass fraction fields

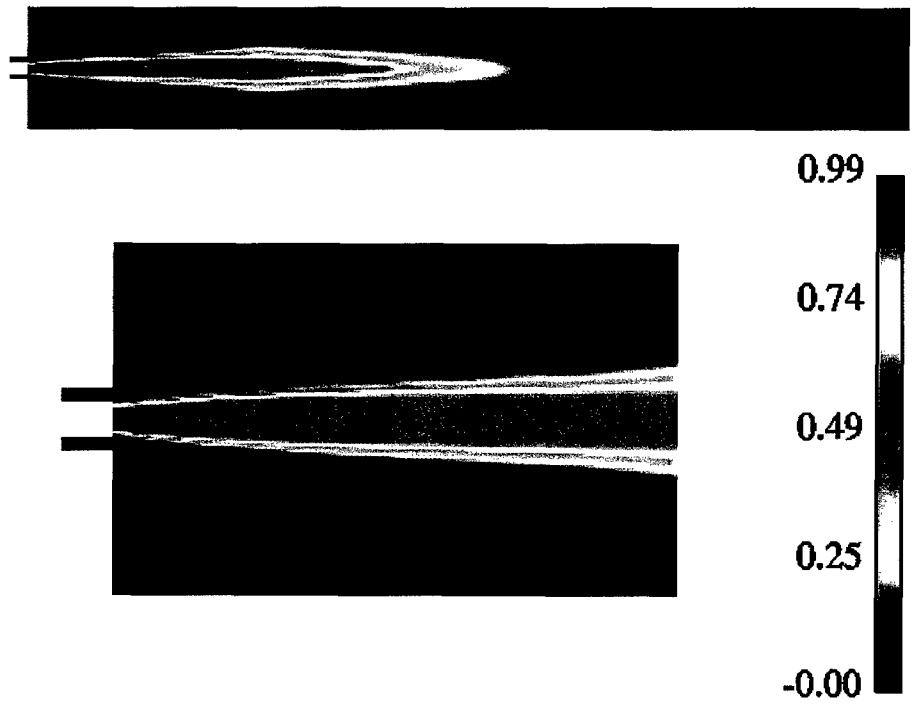

Fig. 6: Gaseous Oxygen mass fraction fields

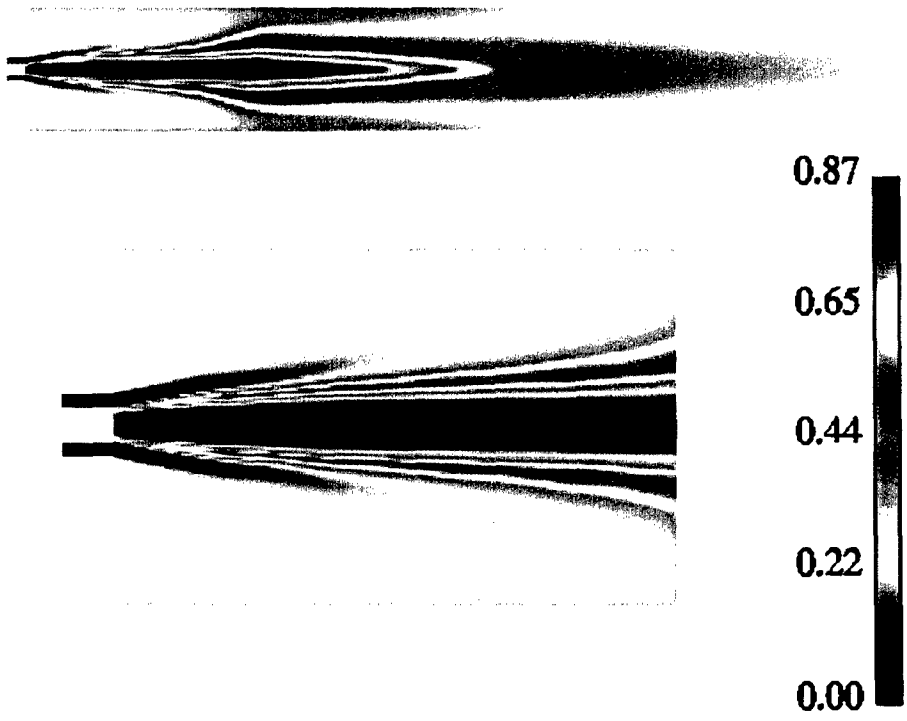

Fig. 7: Water Vapour mass fraction fields

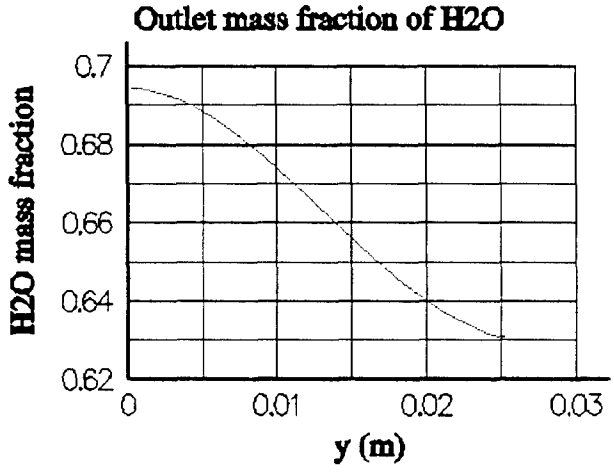

Fig. 8: Axial Water mass fraction at the outlet plane

Fig. 9: Mean reaction rate fields

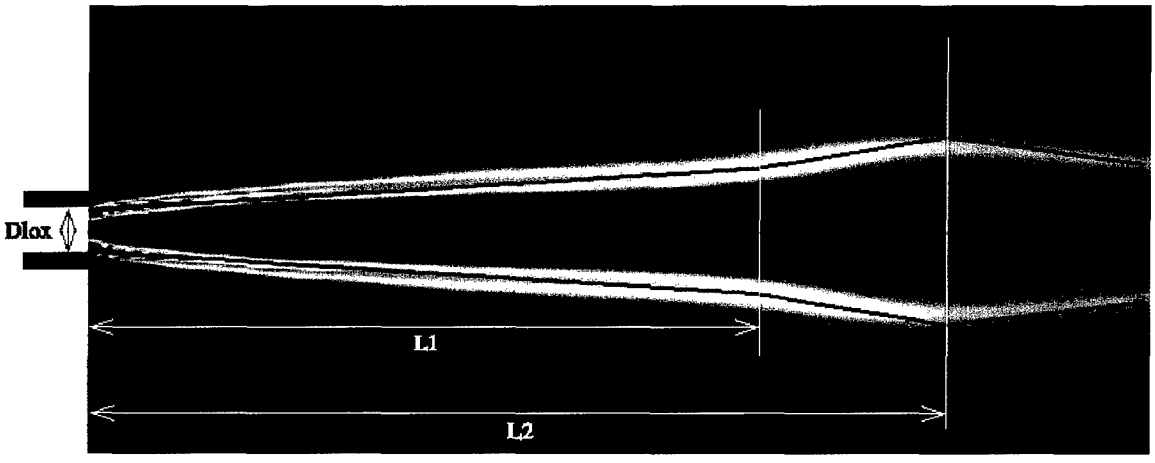

Fig. 10: Characteristic Flame Structure

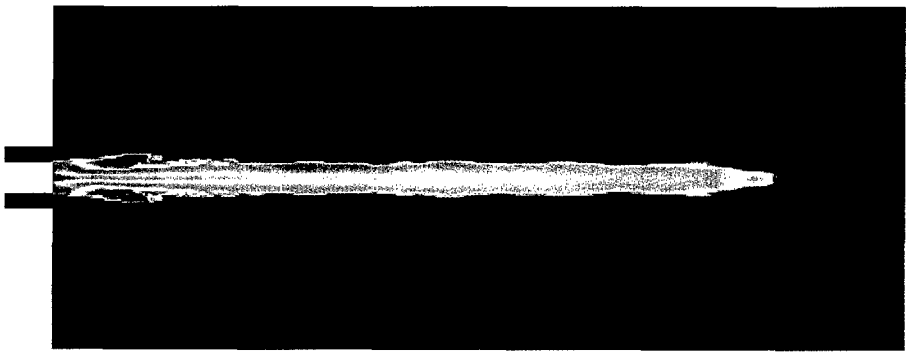

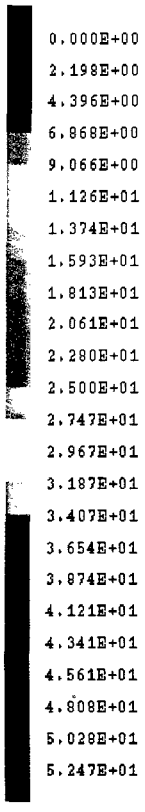

Fig. 11: Droplet Velocity field (m/s)

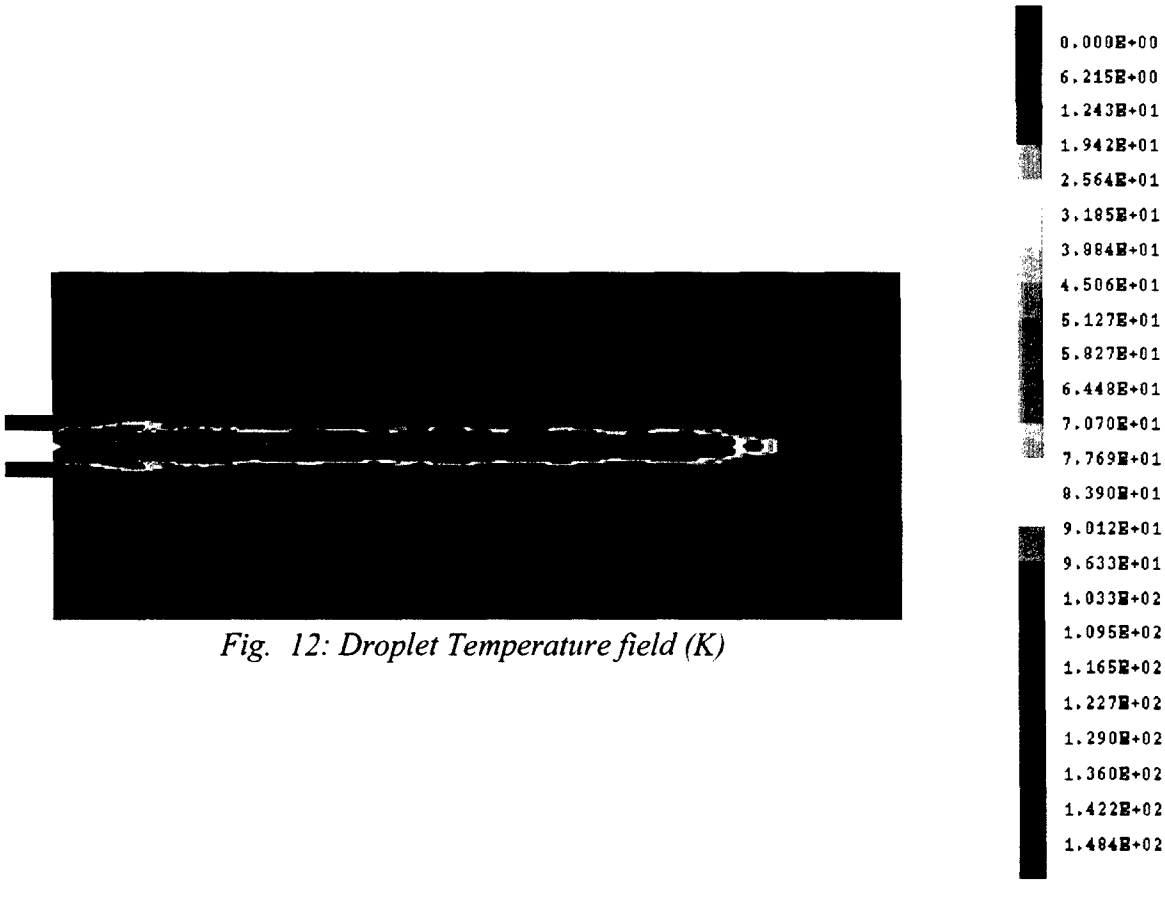

Fig. 12: Droplet Temperature field (K)

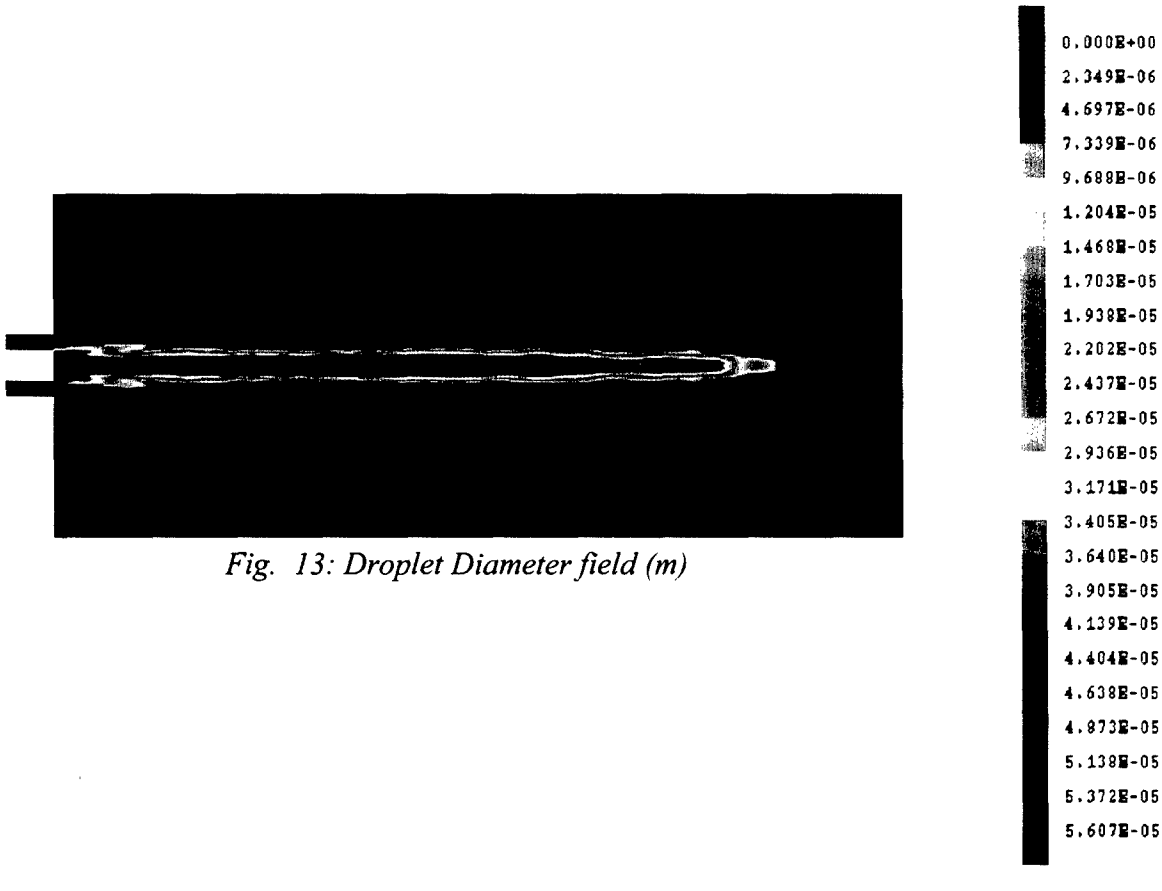

Fig. 13: Droplet Diameter field (m)

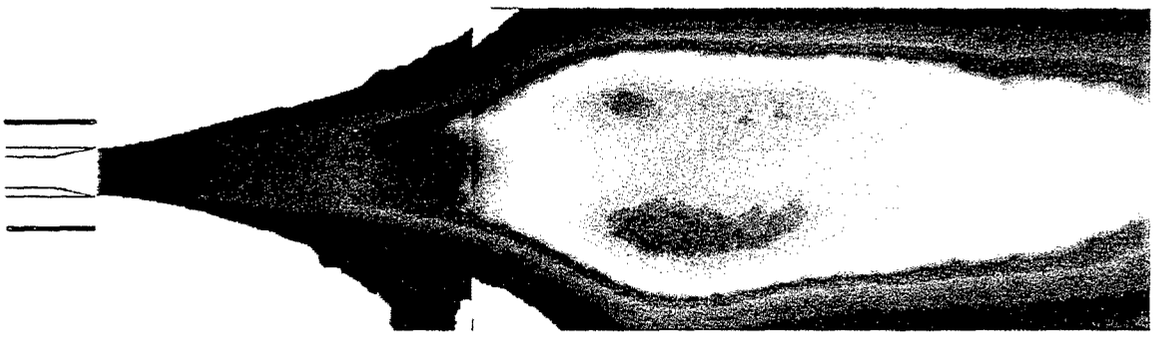

Figure 34: Image d'émission du radical OH^* dans l'UV. 11/03/99, 1er tir et 25/03/99, 1er tir. Point de fonctionnement A. Pression 69 bars. Injecteur sans retrait. Ouverture = 4,5.Gain = 150. Filtrage = 1 UG5, 1 WG305, 1 FNQ027, 1 FNQ015, 1 FNQ007. Durée d'exposition = 3760 μs. Image non normalisée

Fig.14: Experimental data OH emission

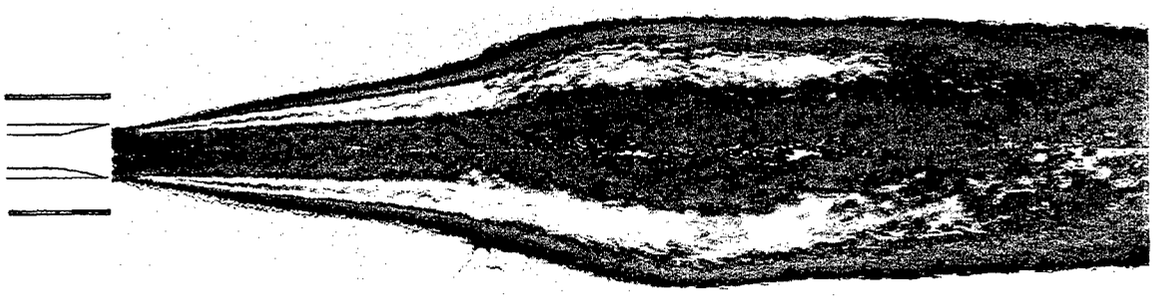

Figure 40: Image par la transformée d'Abel d'émission du radical OH^* dans l'UV. 11/03/99, 1er tir et 25/03/99, 1er tir. Point de fonctionnement A. Pression 69 bars. Injecteur sans retrait. Ouverture = 4,5.Gain = 150. Filtrage = 1 UG5, 1 WG305, 1 FNQ027, 1 FNQ015, 1 FNQ007. Durée d'exposition = 3760 μs. Image non normalisée

Fig.15: Experimental data OH emission (Abel transformed)